Journal of Alloys and Compounds 513 (2012) 251–255

Contents lists available at SciVerse ScienceDirect

Journal of Alloys and Compounds

journal homepage: www.elsevier.com/locate/jallcom

A detailed study of atomic-scale rearrangements in sheared metallic glasses

Francesco Delogu*

Dipartimento di Ingegneria Chimica e Materiali, Università di Cagliari, piazza d'Armi, I-09123 Cagliari, Italy

ARTICLE INFO

Article history:
Received 6 May 2011
Received in revised form 11 October 2011
Accepted 12 October 2011
Available online 20 October 2011

Keywords:
Molecular dynamics
Metallic glasses
Plastic deformation

ABSTRACT

The present study focuses on the molecular dynamics of a model Cu–Ti metallic glass undergoing shear deformation. Numerical findings indicate that deformation induces atomic coordination changes and local irreversible rearrangements. These two processes are intimately connected with each other. In particular, at least one coordination change is observed at the onset of any given rearrangement. It is also shown that coordination changes and rearrangements are preceded by a local increase of atomic stresses as well as by the emergence of local gradients in atomic stress and atomic volume.

1. Introduction

Predicted on a theoretical basis about thirty years ago [1–5], the inelastic distortion of shear transformation zones (STZs) is currently regarded as the elementary mechanistic event underlying the response of metallic glasses (MGs) to shear deformation [6–17]. Although the direct observation of rearranging STZs has not yet been achieved by experiments, local irreversible rearrangements (IRs) ascribable to the operation of STZs have been neatly observed in numerical studies [8–36]. The numerical findings indicate that IRs roughly involve 10–100 atoms [8–36]. These undergo a transition between two relatively low-energy configurations separated by an activation barrier 30–80 kJ mol^{-1} high [8–36]. The non-affine atomic displacements accompanying IRs have been widely employed to identify the structural and mechanical features characterizing the STZs [8–36]. Along this line, it has been recently shown that, under suitable deformation conditions, neighbouring STZs can interact with each other [37–39] and that IRs are sensitive to the local structure [40–43]. In spite of this, no reliable criterion for identifying STZs on a structural basis has been yet identified and the IR activation mechanism is still relatively obscure.

The present work attempts to gain further insight into the above mentioned crucial issues by using molecular dynamics simulations. In particular, the work aims at identifying the common features shared by different IRs by comparing the position of individual atoms before and after the IR of a STZ induced by the MG homogeneous shear deformation. The study focuses on a model $Cu_{50}Ti_{50}$ MG to compare the simulation results with the recent literature on the subject [44].

2. Molecular dynamics simulations

Calculations were carried out by using an embedded-atom method potential [45]. Used in the past to simulate Cu–Ti systems, it is able to satisfactorily reproduce their structural, thermodynamic and mechanical properties [46,47]. Forces were computed within a cut-off radius of about 0.7 nm. Simulations were performed in the isobaric-isothermal ensemble [48,49]. Equations of motion were solved with a fifth-order predictor–corrector algorithm [50] and a time step of 2 fs.

The model $Cu_{50}Ti_{50}$ MG studied in the present work roughly includes 131,000 atoms arranged in a cubic volume with sides about 12.4 nm long. The MG was prepared by quenching the melt from 3000 to 20 K at a rate of 0.02 K ns^{-1} and zero pressure. Periodic boundary conditions (PBCs) were applied along the *x*, *y* and *z* Cartesian directions. According to the Wendt–Abraham method [51], the glass transition occurs at about 620 K, in accordance with previous work [44]. The obtained MG was relaxed for 0.5 ns. The pair distribution function, not shown for brevity, demonstrates that the MG has an amorphous structure. It compares fairly well with the experimental radial distribution function. It follows that the simulated MG has a structure similar to the one of real systems despite the higher quenching rate used in calculations.

Following previous work [28,44,52], rigid reservoirs 1.5 nm thick were created at the top and at the bottom of the simulation cell along the *z* Cartesian direction. PBCs were kept along the *x* and *y* ones. The MG was homogeneously shear deformed along the *x* Cartesian direction by keeping the reservoirs parallel and at constant distance from each other. They were displaced by about

* Tel.: +39 070 675 50 73; fax: +39 070 675 50 67.
E-mail address: delogu@dicm.unica.it

0925-8388/$ – see front matter © 2011 Elsevier B.V. All rights reserved.
doi:10.1016/j.jallcom.2011.10.031

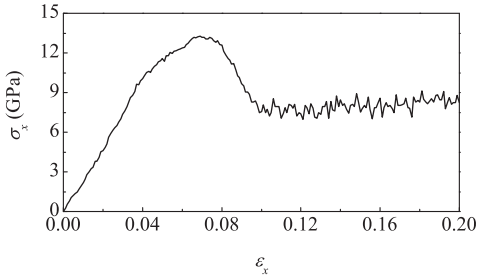

Fig. 1. The average macroscopic stress $\sigma_{macro,x}$ as a function of the average strain $\varepsilon_{macro,x}$.

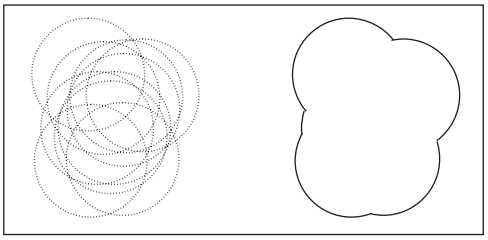

Fig. 2. The volume (right) originating from the overlapping of spherical regions (left) around the atoms involved in coordination changes.

3.1×10^{-3} nm every 100 ps. This resulted in a shear strain increment $\delta\varepsilon_x$ of about 2.5×10^{-4} every 100 ps, corresponding to a shear strain rate of about 2.5×10^{-3} ns^{-1}. This value is lower than the ones generally used in numerical simulations [6,8–36], but remarkably higher than the ones imposed in experiments [6]. Despite this, the results obtained in the present work still provide useful information on the mechanisms operating in real MGs [50].

The shear strain rate has a limited effect on the processes and quantities monitored in the present work. Similar results were obtained at 1×10^{-3} and 5×10^{-3} ns^{-1}. In all of the cases, the deformation was limited to the macroscopic shear strain $\varepsilon_{macro,x}$ range from 0 to 0.2, and performed in the absence of thermostat.

A Voronoi polyhedra space tessellation [53] was used to evaluate the volume Ω of individual atoms. In turn, Ω was used to calculate the average atomic volume Ω_{av} and the average Cu and Ti atomic volumes $\Omega_{Cu,av}$ and $\Omega_{Ti,av}$. Ω was also used to evaluate the atomic stress σ according to standard methods [54]. The macroscopic stress $\sigma_{macro,x}$ along the x Cartesian direction was estimated by averaging σ over all of the MG atoms. The obtained $\sigma_{macro,x}$ values are about 5% lower than the ones resulting from the virial expression [50]. The number n of nearest neighbours of a given atom was set equal to the number of faces of its Voronoi cage.

Following previous work [6,8–21,44,55], the length d of non-affine displacements was used to identify the atoms involved in IRs. For any given atom, d measures the difference between the actual position and the one predicted by affine deformation. It was evaluated on an incremental basis by considering consecutive configurations separated by a single shear strain increment $\delta\varepsilon_x$. Taking into account that the average amplitude of atomic vibrations is equal to about 0.1 Å, a given atom was considered involved in IRs when its non-affine displacement length d was longer than 0.5 Å. This value is in line with the threshold used in previous work [44].

Atomic positions, stress, and volumes were averaged over 5 ps long time intervals.

Three simulations were carried out starting from different initial conditions. The results obtained were substantially the same, with differences in the average quantities of about 1%.

3. Results and discussion

The stress–strain curve typically exhibited by deformed MGs is shown in Fig. 1. The macroscopic shear stress $\sigma_{macro,x}$ undergoes a roughly linear increase from 0 to about 10 GPa as the macroscopic shear strain $\varepsilon_{macro,x}$ increases approximately from 0 to 0.04. Yield takes place in correspondence of $\varepsilon_{macro,x}$ and $\sigma_{macro,x}$ values equal to about 0.07 and 13 GPa, respectively. A steady-state flow regime characterized by $\sigma_{macro,x}$ values oscillating around 8 GPa is attained once $\varepsilon_{macro,x}$ becomes larger than 0.09. The stress–strain curve here obtained is similar to the one exhibited by the same MG at 10 K [44].

Atomic coordination changes occur throughout the deformation process. They appear as localized events involving a number $N_{\Delta n}$ of atoms. Each atom changes Δn nearest neighbours. Such change can regard the number of nearest neighbours, their type, or both.

Coordination changes were studied in detail by defining spherical regions with a radius of 1 nm around each atom of the set of $N_{\Delta n}$ atoms undergoing a coordination change. On the average, individual spherical regions include 280 atoms. However, the $N_{\Delta n}$ atoms are close to each other. Therefore, to a large extent the spherical regions overlap as schematically shown in Fig. 2. Thus, the number of atoms to consider is significantly smaller than $280 \times N_{\Delta n}$. The behaviour of these atoms was investigated by evaluating their stress σ, volume Ω, potential energy u, and non-affine displacement length d. In turn, these quantities were used to calculate the corresponding averages $\bar{\sigma}$, $\bar{\Omega}$, $\bar{u}$, and $\bar{d}$. All of the above mentioned quantities were monitored in the strain interval from $\varepsilon_{macro,x,on} - \Delta\varepsilon_x$ to $\varepsilon_{macro,x,on} + \Delta\varepsilon_x$. Here, $\varepsilon_{macro,x,on}$ is the macroscopic shear strain at which the coordination changes take place and $\Delta\varepsilon_x$ is set equal to 5×10^{-3}.

The average atomic stress $\bar{\sigma}$, potential energy $\bar{u}$, and non-affine displacement length $\bar{d}$ for a representative case in which $N_{\Delta n}$ is equal to 10 are shown in Fig. 3 as a function of the macroscopic shear strain $\varepsilon_{macro,x}$. It can be seen that $N_{\Delta n}$ changes discontinuously from 0 to 10 in a single shear strain increment $\delta\varepsilon_x$. Marked rises in $\bar{\sigma}$ and $\bar{u}$ precede the coordination changes. Once these have taken place, $\bar{\sigma}$ and $\bar{u}$ drop roughly to their initial values. In contrast with the case of $\bar{\sigma}$ and $\bar{u}$, the increase of $\bar{d}$ is much more marked and its subsequent decrease slower. According to the $\bar{d}$ change, the IR associated with coordination changes occurs over a $\varepsilon_{macro,x}$ interval of about 2×10^{-3}. This interval is much longer than the single shear

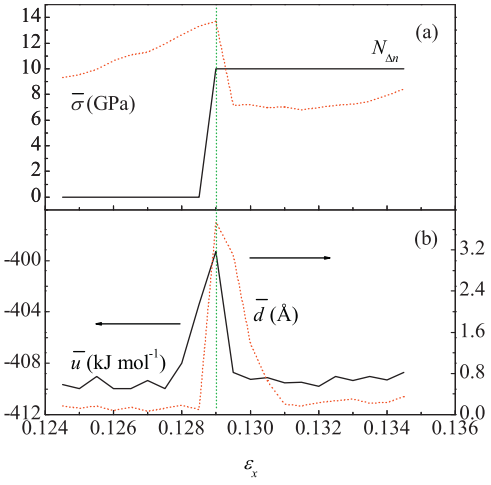

Fig. 3. (a) The number $N_{\Delta n}$ of atoms undergoing a coordination change (black, solid) and the average atomic stress $\bar{\sigma}$ (red, dotted), and (b) the average potential energy $\bar{u}$ per atom (black, solid) and the average non-affine displacement $\bar{d}$ (red, dotted), as a function of the average strain $\varepsilon_{macro,x}$. The vertical dotted line marks the $\varepsilon_{macro,x}$ value of 0.1290 at which coordination changes occur. (For interpretation of the references to colour in this figure legend, the reader is referred to the web version of the article.)

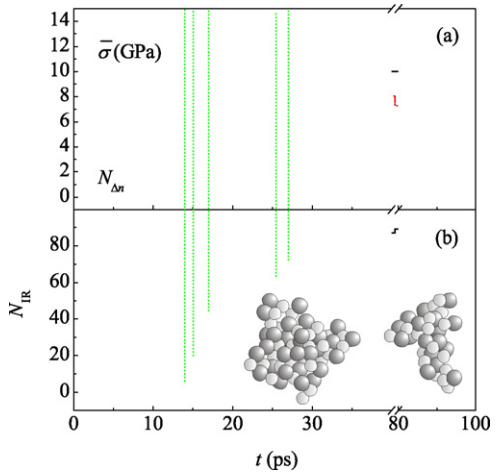

Fig. 4. The number $N_{\Delta n}$ of atoms undergoing a coordination change (black, solid) and the average atomic stress $\bar{\sigma}$ (red, dotted) (a), and the number N_{IR} of atoms participating in the IR (b), as a function of time t. Vertical dotted lines mark the $\bar{\sigma}$ and N_{IR} values corresponding to the $N_{\Delta n}$ increases. The configuration attained after 100 ps by the 89 atoms involved in the IR is also shown in (b) (left), together with the one regarding a different IR involving 52 atoms (right). Light and dark gray indicate Cu and Ti atoms, respectively. Data refer to the IR activated at an average macroscopic strain $\varepsilon_{macro,x}$ of 0.1290. (For interpretation of the references to colour in this figure legend, the reader is referred to the web version of the article.)

strain increment $\delta\varepsilon_x$ of 2.5×10^{-4} over which coordination changes take place.

Contrary to the other quantities, in general the average atomic volume $\bar{\Omega}$ does not undergo significant changes. In the 85% of cases, the difference $\Delta\bar{\Omega}$ between the $\bar{\Omega}$ values before and after the IRs only amounts to about 0.11 ± 0.04 Å^3 at^{-1}. $\bar{\Omega}$ is equal to about 14.53 ± 0.05 Å^3 at^{-1}, a value almost coincident with the average atomic volume Ω_{av}, equal to 14.55 ± 0.04 Å^3 at^{-1}. In the remaining 25% of cases, $\bar{\Omega}$ increases roughly by 1.43 ± 0.08 Å^3 at^{-1}, which corresponds to an average volume increase of about 10%. This value is in line with volume dilatation effects caused by the deformation of MGs [6–17].

Since all the coordination changes take place in the 100 ps following a single shear strain increment $\delta\varepsilon_x$, attention was focused on the dynamics undergone by atoms within such time interval. The number $N_{\Delta n}$ of atoms changing coordination, the average atomic stress $\bar{\sigma}$, and the number N_{IR} of atoms participating in the IR are shown in Fig. 4 as a function of time t. Data in Fig. 4a indicate that $N_{\Delta n}$ increases discontinuously by undergoing a series of rapid rises. Each $N_{\Delta n}$ rise is associated with a marked drop $\Delta\bar{\sigma}$ in the average atomic stress $\bar{\sigma}$. Two groups of coordination changes involving 6 and 4 atoms, respectively can be identified. Within each group, the average time interval Δt separating consecutive coordination changes is about 1.5 ps long. Instead, the average time interval Δt separating the two groups is equal to about 8 ps. It can be seen from Fig. 4b that N_{IR} becomes different from zero, and then the IR starts, only after the first coordination change has occurred. N_{IR} undergoes a smooth monotonic increase and reaches a plateau value of 89 after about 40 ps. The 89 atoms exhibit the relatively compact configuration shown in Fig. 4b. An elongated atomic arrangement observed in a different case is also shown for comparison.

The behaviour described above is common to all the about 5.2×10^4 IRs observed during the MG shear deformation. A detailed statistical analysis of IRs was performed by focusing on the number N_{IR} of atoms involved in a single IR, the number $N_{\Delta n}$ of atoms changing coordination, the number Δn of nearest neighbours changed per atom, the atomic stress drop $\Delta\bar{\sigma}$ at each coordination change, and the time interval Δt separating consecutive coordination changes. The distribution curves $p(N_{IR})$ and $p(N_{\Delta n})$ of N_{IR} and $N_{\Delta n}$, respectively shown in Fig. 5a and b, are asymmetric. The most probable N_{IR} and $N_{\Delta n}$ values range respectively from 80 to 100 and from 6 to 10. As shown in the inset of Fig. 5b, most of the atoms involved in coordination changes change only one nearest neighbour. However, the number Δn of changed nearest neighbours can be as large as 5. The semi-logarithmic plot of $p(\Delta n)$ as a function of Δn, not shown for brevity, is substantially linear. This means that Δn distributes according to an approximately exponential decreasing trend. The statistical distribution $p(\Delta\bar{\sigma})$ of the average atomic stress drop $\Delta\bar{\sigma}$ is shown in Fig. 5c. It can be seen that it is roughly Gaussian, the average $\Delta\bar{\sigma}$ values amounting to about 2.4 GPa. Finally, the inset of Fig. 5c shows that the statistical distribution $p(\Delta t)$ of the time interval Δt separating consecutive coordination changes exhibits bimodal features. Accordingly, the most probable Δt values amount to about 3 and 10 ps.

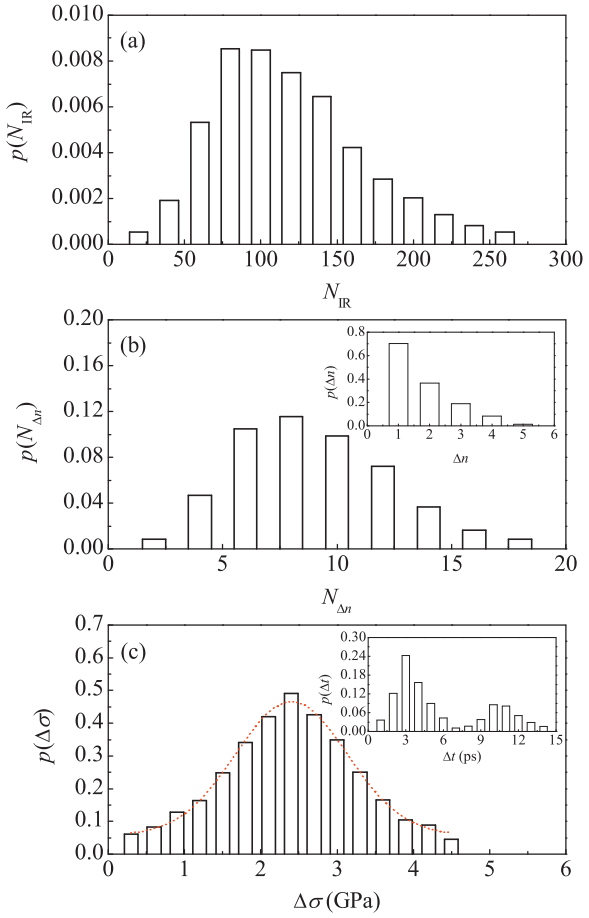

Fig. 5. The statistical distributions p of the number N_{IR} of atoms involved in an IR (a), the number $N_{\Delta n}$ of atoms changing coordination (b), and the atomic stress drops $\Delta\bar{\sigma}$ at each coordination change (c). The $\Delta\bar{\sigma}$ curve in (c) has been best-fitted by a Gaussian function, also shown. The insets in (b) and (c) show, respectively, the statistical distribution p of the number Δn of nearest neighbours changed per atom and of the time interval Δt separating consecutive coordination changes.

The observed bimodality of $p(\Delta t)$ must be connected with the different time scales governing coordination changes. Individual coordination changes typically occur in about 0.5 ps. Two or more coordination changes taking place during the same IR can group in a cascade, which can be defined as a sequence of coordination changes separated by relatively short time intervals. These short time intervals originate the first peak of $p(\Delta t)$. When the number $N_{\Delta n}$ of coordination changes is relatively small, a single cascade is generally observed. However, $N_{\Delta n}$ can be as large as 18. Large $N_{\Delta n}$ values typically give rise to two or three cascades, separated by

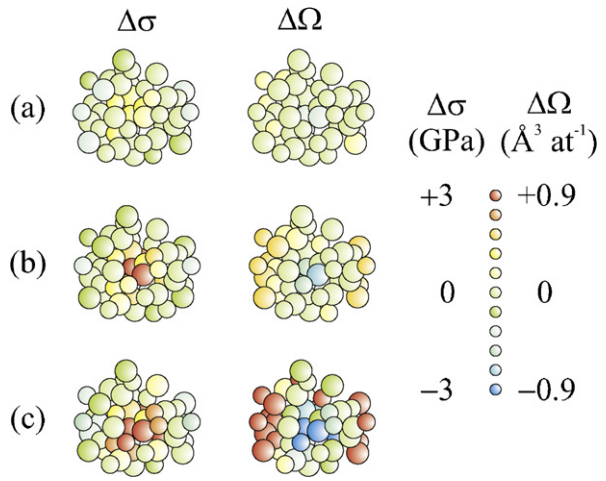

Fig. 6. Cross-sectional views of the atomic configurations of a set of atoms involved in an IR starting at an average strain $\varepsilon_{macro,x}$ value of 0.1030. The differences $\Delta\sigma$ (left) and $\Delta\Omega$ (right) are indicated by the colour codes shown on the right. The atomic configurations are taken at the average macroscopic strain $\varepsilon_{macro,x}$ values of 0.0930 (a), 0.0990 (b) and 0.1025 (c). Only a single strain increment $\delta\varepsilon_x$ separates the latter value from the one of 0.1030 at which the coordination changes occur.

relatively long time intervals. These long time intervals originate the second peak of $p(\Delta t)$.

The statistical analysis performed only pointed out a generic relationship between $N_{\Delta n}$ and N_{IR}. In particular, the larger the number $N_{\Delta n}$ of atoms affected by coordination changes, the larger the number N_{IR} of atoms participating in the IR. Apart from this, no other correlation was found among the monitored quantities. The height of stress drops $\Delta\bar{\sigma}$ and the length of time intervals Δt do not correlate with $N_{\Delta n}$ or N_{IR}. Furthermore, the $N_{\Delta n}$ and N_{IR} values change irregularly from one IR to the successive one, and this is also true for $\Delta\bar{\sigma}$ and Δt values.

A feature common to all of the observed IRs emerges only when the differences $\Delta\sigma = \sigma - \sigma_{av}$ and $\Delta\Omega = \Omega - \Omega_{av}$ are calculated. Here, σ_{av} and Ω_{av} are the average atomic stress and volume of the IR atoms at a given macroscopic shear strain $\varepsilon_{macro,x}$. The atomic volume differences $\Delta\Omega$ were evaluated by distinguishing between Cu and Ti, which have quite different average volumes $\Omega_{Cu,av}$ and $\Omega_{Ti,av}$. The former amounts to about 12.4 Å^3 at^{-1}, whereas the latter is equal to about 18.6 Å^3 at^{-1}.

The $\Delta\sigma$ and $\Delta\Omega$ values have been used to describe the evolution of local conditions undergone by the atoms involved in IRs when the macroscopic shear strain $\varepsilon_{macro,x}$ increases. Information relative to such conditions can be visualized by using a colour code to indicate $\Delta\sigma$ and $\Delta\Omega$ values. An example is given in Fig. 6, which shows three cross-sectional views of the configurations reached by the atoms involved in the IRs already analyzed in detail in Figs. 3 and 4. Data refer to increasing macroscopic shear strain $\varepsilon_{macro,x}$ values. It can be seen that the stress experienced by the atoms located in the core of the region occupied by the atoms involved in the IR increases as $\varepsilon_{macro,x}$ increases, whereas their volume correspondingly decreases. The outer atoms exhibit opposite trends. The observed $\Delta\sigma$ and $\Delta\Omega$ differences suddenly disappear as the IR occurs.

The atomic volume differences $\Delta\Omega$ between inner and outer atoms were further investigated by studying their spatial distribution $\Delta\Omega(\Delta r)$. For any given IR, the atom experiencing the highest stress σ in the strain increment $\delta\varepsilon_x$ immediately preceding the coordination changes was identified. Concentric spherical shells 0.05 nm thick were defined around such atom. The volume differences $\Delta\Omega$ shown by the atoms inside each shell were summed and normalized to their number. The $\Delta\Omega(\Delta r)$ curves for IRs occurring at different $\varepsilon_{macro,x}$ values were compared by using a relative scale.

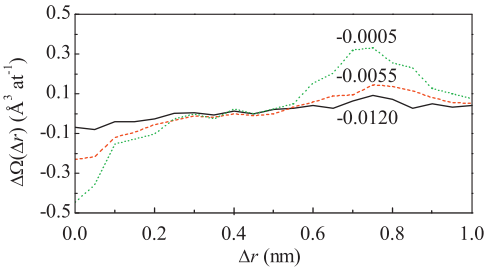

Fig. 7. The spatial distribution $\Delta\Omega(\Delta r)_{av}$ of the volume differences for the atoms inside spherical shells as a function of the shell distance Δr from the most stressed atom. Data refer to average macroscopic strain differences $\Delta\varepsilon_{macro,x}$, equal to −0.0120 (solid line, black), −0.0055 (dashed line, red), and −0.0005 (dotted line, green). (For interpretation of the references to colour in this figure legend, the reader is referred to the web version of the article.)

This scale is based on the values of $\Delta\varepsilon_{macro,x} = \varepsilon_{macro,x} - \varepsilon_{macro,x,on}$, referred to the macroscopic shear strain $\varepsilon_{macro,x,on}$ at which the first coordination change takes place. $\Delta\varepsilon_{macro,x}$, is negative for the macroscopic shear strain values preceding the IR onset, and positive for others. The cumulative spatial distribution $\Delta\Omega(\Delta r)$ was calculated by combining the $\Delta\Omega(\Delta r)$ values of different IRs sharing the same macroscopic shear strain difference $\Delta\varepsilon_{macro,x}$. The $\Delta\Omega(\Delta r)$ values for the different IRs were summed and normalized to the number of IRs.

The $\Delta\Omega(\Delta r)_{av}$ curves obtained at different $\Delta\varepsilon_{macro,x}$ values are plotted in Fig. 7 as a function of the distance Δr of each shell from the central atom. $\Delta\Omega(\Delta r)_{av}$ is quite flat for large, negative, $\Delta\varepsilon_{macro,x}$ values. As $\Delta\varepsilon_{macro,x}$ increases, i.e. as the set of atoms approaches the onset of the IR, $\Delta\Omega(\Delta r)_{av}$ takes negative values at short Δr distances and positive values at relatively long distances. This indicates an atomic volume compression due to locally high atomic stresses at short distances, and an atomic volume expansion at long ones. Thus, a gradient in the atomic volume appears inside the sets of atoms involved in the IRs. This is a characteristic feature of IRs, irrespective of their size and of the strain at which they occur.

The numerical findings indicate that the response of MGs to shear deformation is significantly inhomogeneous. In fact, only a few regions of the whole MG volume are instantaneously involved in IRs. The correlation between the onset of IRs and the occurrence of atomic coordination changes further supports the hypothesis that the MG volume includes local structures with different propensity to IR. It is interesting to note that similar conjectures are discussed also in connection with fragility scenarios for glass-forming liquids [56,57].

Before concluding, a comment on the thermal behaviour of the deformed MG is necessary. The atoms undergoing IRs throughout the deformation process undergo instantaneous temperature rises on the order of 100 K. On the average, such temperature spikes disappear in about 200 ps. At the end of simulations, the average MG temperature has increased by only 5 K. This confirms that only a relatively small number of atoms is involved in IRs. The amount of energy dissipated as heat is correspondingly small.

The 5 K temperature rise is slightly smaller than the ones observed in other simulation works for similar deformation degrees. For example, in the case of a Ni–Zr system the average temperature increased by about 40 K [53]. However, such system was deformed at 2.4 and 0.2 ns^{-1}, which are quite higher than the strain rate of about 2.5×10^{-3} ns^{-1} used in the present work. In addition, simulations were carried out at 100 K [53], whereas the present Cu–Ti system was studied at 20 K. In principles, these differences can be at the basis of the different temperature rises observed.

In this regard, it is worth noting that the amount of energy dissipated crucially depends on the deformation conditions [6].

Experimental and theoretical studies suggest that a significant temperature increase must be expected whenever strain rates are high enough to assure almost adiabatic deformation processes [6,9,10]. Numerical simulations seems to be particularly suited to study adiabatic deformation, being the strain rates employed quite higher than experimental ones [6,9,10]. However, it must be noted that the shear bands formed during experiments are about 10–100 nm thick and appear in MG samples with volumes of 1–10 cm^3 deformed for time intervals 10–100 s long [6–17,58,59]. The deformation conditions accessible to numerical studies are significantly far from these, and it cannot be reasonably expected that the temperature rises observed in experiments are correctly reproduced [6–17]. In addition, the temperature at which deformation is carried out plays a fundamental role in shear localization processes [6–17]. In particular, low temperatures greatly facilitate the operation of individual STZs and the localization of the STZ activity in small regions [6–17,37–39]. Also, the number of STZs activated is in general smaller [6–17]. The results obtained in the present work suggest that temperature rises can be smaller at lower temperatures. The lack of direct experimental measurements of the temperature rise in shear bands formed by low-temperature deformation limits our understanding of this issue.

4. Conclusions

The shear deformation of MGs is mediated by the occurrence of IRs. Each IR involves a relatively small region and is preceded by a coordination change. Before the coordination change occurs, the atoms involved in the IR undergo a local stress increase, followed by a sudden stress drop every time a coordination change occurs. Each region involved in IRs exhibits gradients in atomic stresses and volumes. The atoms in the inner part of the region experience higher stresses, whereas the outer atoms experience lower stresses. At the same time, the atoms in the inner part exhibit a smaller volume, whereas the outer ones are characterized by a larger volume.

Further studies are needed to throw light on the intimate details of the mechanisms leading to the onset of individual IRs.

Acknowledgements

The author is indebted with Prof. M. Atzmon, Departments of Materials Science and Engineering and of Nuclear Engineering and Radiological Sciences, University of Michigan, Ann Arbor (MI, USA), for useful discussions. Financial support has been given by the University of Cagliari. A. Ermini, ExtraInformatica s.r.l., is gratefully acknowledged for his kind assistance.

References

[1] S.A. Argon, H.Y. Kuo, Mater. Sci. Eng. 39 (1979) 101.
[2] S.A. Argon, J. Phys. Chem. Solids 43 (1982) 945.
[3] V.V. Bulatov, S.A. Argon, Model. Simul. Mater. Sci. Eng. 2 (1994) 167.
[4] V.V. Bulatov, A.S. Argon, Model. Simul. Mater. Sci. Eng. 2 (1994) 185.
[5] V.V. Bulatov, A.S. Argon, Model. Simul. Mater. Sci. Eng. 2 (1994) 203.
[6] C.A. Schuh, T.C. Hufnagel, U. Ramamurty, Acta Mater. 55 (2007) 4067.
[7] A.R. Yavari, J.J. Lewandowski, J. Eckert, MRS Bull. 32 (2007) 611.
[8] M. Martin Trexler, N.N. Thadhani, Prog. Mater. Sci. 55 (2010) 759.
[9] Y.Q. Cheng, E.E. Ma, Prog. Mater. Phys. 56 (2011) 379.
[10] S. Takeuchi, K. Edagawa, Prog. Mater. Phys. 56 (2011) 785.
[11] T. Egami, Intermetallics 14 (2006) 882.
[12] A. Dubach, F.H. Dalla Torre, J.F. Löffler, Acta Mater. 57 (2009) 881.
[13] X.J. Liu, G.L. Chen, F. Li, X.D. Hui, Z.P. Lu, F. Ye, C.Y. Liu, Intermetallics 18 (2010) 2333.
[14] K.-W. Park, Y. Shibutani, M.L. Falk, B.-J. Lee, J.-C. Lee, Scr. Mater. 63 (2010) 231.
[15] H.G.E. Hentschel, S. Karmakar, E. Lerner, I. Procaccia, Phys. Rev. Lett. 104 (2010) 025501.
[16] H.B. Yu, W.H. Wang, H.Y. Bai, Y. Wu, M.W. Chen, Phys. Rev. B 81 (2010) 220201.
[17] K.-W. Park, H. Park, E. Fleury, Mater. Sci. Eng. A 528 (2011) 5319.
[18] M.L. Falk, J.S. Langer, Phys. Rev. E 57 (1998) 7192.
[19] J.S. Langer, Phys. Rev. E 64 (2001) 011504.
[20] J.S. Langer, Scr. Mater. 54 (2006) 375.
[21] M.L. Manning, J.S. Langer, L.M. Carlson, Phys. Rev. E 76 (2007) 056106.
[22] A. Lemaître, Phys. Rev. Lett. 89 (2002) 195503.
[23] M.L. Falk, Phys. Rev. B 60 (1999) 7062.
[24] Y. Shi, M.L. Falk, Phys. Rev. Lett. 95 (2006) 095502.
[25] Y. Shi, M.B. Katz, H. Li, M. Falk, Phys. Rev. Lett. 98 (2007) 185505.
[26] C.A. Schuh, A.C. Lund, Nat. Mater. 2 (2003) 449.
[27] A.C. Lund, C.A. Schuh, Acta Mater. 51 (2003) 5399.
[28] Q.K. Li, M. Li, Appl. Phys. Lett. 88 (2006) 241903.
[29] E.A. Jagla, Phys. Rev. A 76 (2007) 046119.
[30] M.L. Falk, C.E. Maloney, Eur. Phys. J. B 75 (2010) 405.
[31] M. Falk, J.S. Langer, Annu. Rev. Condens. Matter Phys. 2 (2011) 353.
[32] C. Fusco, T. Albaret, A. Tanguy, Phys. Rev. E 82 (2010) 066116.
[33] A. Lemaître, C. Caroli, Phys. Rev. Lett. 103 (2009) 065501.
[34] S.G. Mayr, Phys. Rev. B 79 (2009) 060201.
[35] C.L. Rountree, D. Vandembroucq, M. Talamali, E. Bouchaud, S. Roux, Phys. Rev. Lett. 102 (2009) 195501.
[36] M. Tsamados, A. Tanguy, C. Goldenberg, J.-L. Barrat, Phys. Rev. E 80 (2009) 026112.
[37] D. Rodney, C.A. Schuh, Phys. Rev. Lett. 102 (2009) 235503.
[38] D. Rodney, C.A. Schuh, Phys. Rev. B 80 (2009) 184203.
[39] E.R. Homer, D. Rodney, C.A. Schuh, Phys. Rev. B 81 (2010) 064204.
[40] H.W. Sheng, W.K. Luo, F.M. Alamgir, J.M. Bai, E. Ma, Nature 439 (2006) 419.
[41] L. Zhang, Y.Q. Cheng, A.J. Cao, J. Xu, E. Ma, Acta Mater. 57 (2009) 1154.
[42] Y.Q. Cheng, A.J. Cao, E. Ma, Acta Mater. 57 (2009) 3253.
[43] A.J. Cao, Y.Q. Cheng, E. Ma, Acta Mater. 57 (2009) 5146.
[44] M. Neudecker, S.G. Mayr, Acta Mater. 57 (2009) 1437.
[45] M.S. Daw, M.I. Baskes, Phys. Rev. B 29 (1984) 6443.
[46] M.J. Sabochick, N.Q. Lam, Phys. Rev. B 43 (1991) 5243.
[47] N.Q. Lam, P.R. Okamoto, M. Li, J. Nucl. Mater. 251 (1997) 89.
[48] H.C. Andersen, J. Chem. Phys. 72 (1980) 2384.
[49] S. Nosè, J. Chem. Phys. 81 (1984) 511.
[50] M.P. Allen, D. Tildesley, Computer Simulation of Liquids, Clarendon Press, Oxford, 1987.
[51] H.R. Wendt, F.F. Abraham, Phys. Rev. Lett. 41 (1978) 1244.
[52] F. Delogu, Phys. Rev. Lett. 100 (2008) 075901.
[53] J.L. Finney, Proc. R. Soc. Lond., Ser. A 319 (1970) 495.
[54] Z.S. Basinski, M.S. Duesberry, R. Taylor, Can. J. Phys. 49 (1971) 2160.
[55] C.E. Maloney, A. Lemaître, Phys. Rev. E 74 (2006) 016118.
[56] C. Zhang, L. Hu, Y. Yue, J.C. Mauro, J. Chem. Phys. 133 (2010) 014508.
[57] S. Wei, I. Gallino, F. Busch, C.A. Angell, Nat. Phys. 7 (2011) 178.
[58] Y. Zhang, A.L. Greer, Appl. Phys. Lett. 89 (2006) 071907.
[59] L. Battezzati, D. Baldissin, Scr. Mater. 59 (2008) 223.